J Braz. Soc. Mech. Sci. Eng. (2016) 38:2435–2448
DOI 10.1007/s40430-016-0514-x

TECHNICAL PAPER

# Cutting temperature analysis considering the improved Oxley's predictive machining theory

**Mehmet Aydın**[1]

Received: 13 August 2015 / Accepted: 22 February 2016 / Published online: 9 March 2016


**Abstract** This article deals with the identification of the temperature distributions in the chip, tool and workpiece based on orthogonal cutting data estimated analytically from the improved version of the Oxley's machining theory, including the strain-hardening constant ($n_{eq}$) and the Johnson–Cook (JC) flow stress equation. The improved Oxley's machining theory and thermal model were separately considered to compute temperature distributions. The initial parameters ($\delta$, $C_0$, $\phi$) and temperature factors ($\eta$, $\psi$) of Oxley's model were optimized to improve the computation efficiency and estimation accuracy. The thermal model considers the effects of the primary and secondary heat sources. The primary heat source was depicted as a uniformly acting oblique band. The secondary heat source was modeled by applying non-uniform distribution of the heat partition ratio. The estimated results were compared with the published results of an experimental investigation in machining of AISI 1045 steel. It was found that the results of the improved Oxley's model were closer to the experimental values than the outcomes of its extended version. A detailed set of the temperature distributions was introduced and the estimated temperature values were in good agreement with the experimental results.

**Keywords** Heat source · Machining theory · Orthogonal cutting · Temperature modeling

Technical Editor: Márcio Bacci da Silva.

✉ Mehmet Aydın
mehmet.aydin@bilecik.edu.tr

[1] Department of Industrial Product Design, Bilecik Şeyh Edebali University, 11210 Bilecik, Turkey

**List of symbols**

| | |
|---|---|
| $a$ | Thermal diffusivity |
| $A$, $B$, $C$, $m$, $n$ | Constants of the JC model |
| $B_{i,chip}$, $B_{i,tool}$ | Heat partition ratios for chip and tool |
| $C_0$ | Strain rate constant along AB |
| $E_j$, $E_k$ | Quadratic sum of relative errors |
| $f$ | Feed rate |
| $F$, $N$ | Frictional and normal forces at the tool/chip interface |
| $F_c$, $F_f$ | Cutting and feed forces |
| $F_{c,E}$, $F_{f,E}$ | Cutting and feed forces estimated from extended Oxley's model |
| $F_{ci}$, $F_{c,ij}$, | Measured and estimated cutting forces |
| $F_{c,I}$, $F_{f,I}$ | Cutting and feed forces estimated from the improved Oxley's model |
| $F_{fi}$, $F_{f,ij}$ | Measured and estimated feed forces |
| $F_s$, $F_n$ | Shear and normal forces at $AB$ |
| $k_{AB}$, $k_{chip}$ | Shear flow stresses of $AB$ and chip |
| $K_0$ | Zero-order Bessel function |
| $l_{AB}$, $l_p$, $l_c$ | Shear plane, sticking region and tool–chip contact lengths |
| $l_i$ | Position of differential element $dl_i$ |
| $n_{eq}$ | Strain-hardening constant |
| $M$ | Point for calculating temperature increase |
| $q_{shear}$, $q_{friction}$, $q_{induced}$ | Shear, friction and induced heat source intensities |
| $R$ | Resultant force |
| $R_T$ | Thermal number |
| $R_1$, $R_2$ | Distance between heat source and point $M$ |
| $t_c$ | Chip thickness |
| $t_{ci}$, $t_{c,ij}$ | Measured and estimated chip |

| | |
|---|---|
| | thicknesses |
| $t_{c,I}$, $t_{c,E}$ | Chip thicknesses calculated from improved and extended Oxley's models |
| $S$ | Specific heat |
| $T$, $T_m$ | Instantaneous and melting temperatures of workpiece |
| $T_{AB}$ | Average temperature of $AB$ |
| $T_{int}$, $T_{M,int}$ | Average and maximum temperatures of tool/chip interface |
| $T_{inti}$, $T_{int,ij}$ | Measured and estimated average temperatures along the tool/chip interface |
| $T_M$ | Temperature increase at point $M$ |
| $T_r$ | Room temperature |
| $V$, $V_c$, $V_{ch}$, $V_s$ | Velocity of shear plane, cutting speed, chip and shear velocities |
| $w$ | Width of cut |
| $x_i$, $y_i$ | Positions of differential elements $dx_i$ and $dy_i$ |
| $X$, $z$ | Coordinates of point $M$ used for temperature calculation |
| $\alpha$, $\phi$, $\varphi$ | Rake, shear and oblique angles |
| $\beta_a$ | Global friction angle |
| $\beta_T$ | Ratio of heat transferred into the workpiece |
| $\gamma_{AB}$, $\gamma_{int}$ | Shear strains of $AB$ and the tool/chip interface |
| $\dot{\gamma}_{AB}$, $\dot{\gamma}_{int}$ | Shear strain rates of $AB$ and the tool/chip interface |
| $\delta$ | Strain rate constant of the tool/chip interface |
| $\Delta F_c$ | Relative difference between outcomes $F_c$ estimated from improved and extended Oxley's models |
| $\Delta F_f$ | Relative difference between outcomes $F_f$ estimated from improved and extended Oxley's models |
| $\Delta t_c$ | Relative difference between outcomes $t_c$ estimated from improved and extended Oxley's models |
| $\Delta T_c$ | Average temperature increase in the chip |
| $\Delta T_{M,c}$, $\Delta T_{M,t}$ | Maximum temperature increases in the chip and tool |
| $\varepsilon$, $\dot{\varepsilon}$ | Equivalent strain and strain rate |
| $\varepsilon_{AB}$, $\dot{\varepsilon}_{AB}$ | Equivalent strain and strain rate at $AB$ |
| $\varepsilon_E$ | Absolute error between outcomes measured and estimated from the extended model |
| $\varepsilon_{int}$, $\dot{\varepsilon}_{int}$ | Equivalent strain and strain rate at the tool/chip interface |
| $\varepsilon_I$ | Absolute error between outcomes measured and estimated from the improved model |
| $\varepsilon T_c$ | Relative difference between average temperatures in the chip for tools with negative and positive rake angles |
| $\varepsilon T_{int,c}$ | Relative difference between the estimated maximum chip temperature and measured maximum tool/chip interface temperature |
| $\varepsilon T_{int,t}$ | Relative difference between the estimated maximum tool temperature and measured maximum tool/chip interface temperature |
| $\dot{\varepsilon}_0$ | Reference strain rate |
| $\eta$, $\psi$ | Shear zone and tool/chip interface temperature factors |
| $\eta_k$, $\psi_k$ | Estimated values of temperature factors $\eta$ and $\psi$ |
| $\theta$ | Angle between $R$ and $AB$ |
| $\lambda_c$, $\lambda_t$ | Thermal conductivities of chip and tool |
| $\mu$, $\mu_{local}$ | Global and local friction coefficients |
| $\xi$ | Exponential constant |
| $\rho$ | Density |
| $\sigma_{AB}$ | Flow stress at $AB$ |
| $\sigma_N$, $\sigma'_N$ | Normal stresses of tool/chip interface and point B |
| $\tau_{int}$, $\tau_{st}$ | Shear stresses of tool/chip interface and sticking zone |

## 1 Introduction

Models of the machining process provide a fundamental understanding for quantitative analysis of cutting forces [1, 2], stresses [3], cutting temperatures [4], tool wear [5], dimensional accuracy [6, 7] and surface roughness [8] in practical operating conditions. Thus, analytical and thermal models of machining processes including many phenomena such as plasticity, friction and heat generation have attracted many researchers' attentions.

Several analytical approaches have been suggested to estimate force, stress and temperature intensities in deformation zones. Oxley [9] built a parallel-sided shear zone theory, depicted as Oxley's theory, for estimating machining outcomes. Oxley's theory uses the thermal properties and flow stress of workpiece material to acquire process outputs. Adibi-Sedeh et al. [10] modified Oxley's theory to

estimate force and temperature intensities using a variety of material models. They studied the influence of strain at the tool/chip interface and stated that the JC model [11] provided the most successful performance in estimating cutting forces. Özel and Zeren [12] suggested some changes to Oxley's theory by considering the non-uniform distribution of the normal stress and the secondary shear zone as triangular in shape. Lalwani et al. [13] included the JC model into Oxley's theory to estimate the force and temperature intensities with a simpler approach. Xiong et al. [14] improved the algorithm of the extended Oxley's model [13] for computing cutting forces, feed forces and chip thicknesses through better accuracy and efficiency.

Most studies on thermal aspects of machining processes have been performed to measure cutting temperatures [15]. Temperature modeling in the cutting zone is highly significant, because cutting temperatures affect the tool life, workpiece surface quality and chip formation. Komanduri and Hou [16–18] introduced thermal models for machining process by considering the primary and secondary heat sources with border circumstances and imaginary heat sources in a semi-infinite medium. Karpat and Özel [19] incorporated Komanduri and Hou's thermal model into Oxley's model to estimate forces, stresses and temperatures. To improve Oxley's machining model, Huang and Liang [20] determined temperature distributions at primary and secondary deformation zones from Huang and Liang's approach [21] and used an enhanced JC model to estimate cutting forces in hard turning with CBN tools. They did not study the influence of strain at the secondary shear zone. Chen et al. [22] modified Oxley's model for different materials by applying the JC model and a thermal approximation. Li et al. [23] established a modified thermal model for estimating cutting temperatures in dry orthogonal cutting. In their model, they used Komanduri and Hou's heat source method. Most of the researches cited have addressed the extension of Oxley's theory with different approaches for engineering materials. No effort has been made to determine the temperature distributions, which contribute as the main factor to evaluate tool wear rate in machining, by carrying out the improvement of Oxley's machining theory. Further, none of these have completely and clearly considered temperature distributions in the chip formation process.

The objective of the study is to identify temperature distributions of the chip, cutting tool and workpiece by considering cutting data estimated analytically from the improved version of Oxley's model extended by applying the strain-hardening constant ($n_{eq}$). The improvements to Oxley's theory are made by optimizing the initial values of model parameters ($\delta$, $C_0$, $\phi$) and temperature factors ($\eta$, $\psi$) to enhance the estimation accuracy and efficiency. The suggested approach can contribute to express the influence of the improved Oxley's model on temperature distributions by considering the cutting parameters and configurations.

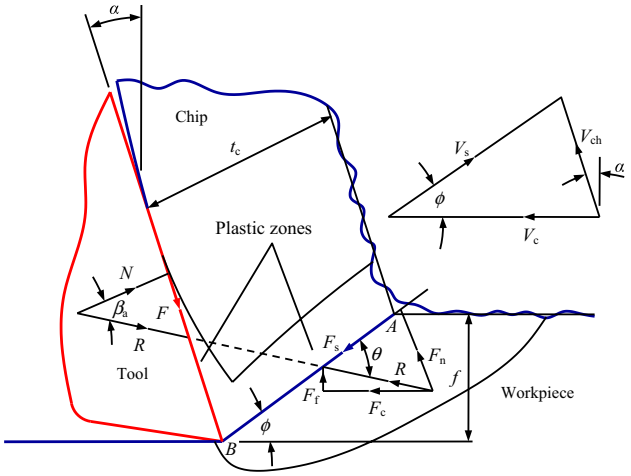


**Fig. 1** Chip formation model for orthogonal machining [9]

## 2 Improved Oxley's machining model

Oxley's model is a machining approach acquired through the slip-line field analysis and strain rate analysis of flow fields. Plain strain and steady-state circumstances are supposed for a continuous chip formation with a sharp tool, as seen in Fig. 1 [9].

Based on the acquired global optimal solution by Xiong et al. [14], the initial values of strain rate constant of tool/chip interface ($\delta$), strain rate constant of shear zone ($C_0$) and shear angle ($\phi$) are adopted as 0.01, 1, and 15° to increase the estimation efficiency and satisfy the force equilibrium for AISI 1045 steel, respectively. $\phi$ is iteratively searched until the shear stress at the tool/chip interface ($\tau_{int}$) meets the shear flow stress in the chip at the tool/chip interface ($k_{chip}$). $C_0$ is determined when the normal stress at the tool/chip interface ($\sigma_N$) equals the normal stress acting at point $B$ ($\sigma'_N$). $\delta$ is found by considering the minimum cutting force principle.

### 2.1 Flow stress model

To describe the workpiece material behavior, the JC flow stress equation [11] is integrated into Oxley's theory, represented by

$$\sigma = (A + B(\varepsilon)^n)\left(1 + C\,\mathrm{In}\frac{\dot{\varepsilon}}{\dot{\varepsilon}_0}\right)\left(1 - \left(\frac{T - T_r}{T_m - T_r}\right)^m\right), \tag{1}$$

where $(T - T_r)/(T_m - T_r)$ is the normalized temperature and denoted by $T^*$.

### 2.2 Shear plane

The shear flow stress ($k_{AB}$), strain ($\varepsilon_{AB}$) and strain rate ($\dot{\varepsilon}_{AB}$) along the shear plane ($AB$) are calculated according to the von Mises criterion [13]

$$\begin{cases} k_{AB} = \frac{1}{\sqrt{3}}(A + B\varepsilon_{AB}^{n})\left(1 + C\,\mathrm{In}\frac{\dot{\varepsilon}_{AB}}{\dot{\varepsilon}_0}\right)\left(1 - \left(\frac{T_{AB}-T_r}{T_m-T_r}\right)^{m}\right), \\ \varepsilon_{AB} = \frac{\gamma_{AB}}{\sqrt{3}} = \frac{\cos\alpha}{2\sqrt{3}\sin\phi\cos(\phi-\alpha)}, \\ \dot{\varepsilon}_{AB} = \frac{\dot{\gamma}_{AB}}{\sqrt{3}} = C_0\frac{V_s}{\sqrt{3}l_{AB}}, \end{cases} \tag{2}$$

where $A = 553.1$ MPa, $B = 600.8$ MPa, $n = 0.234$, $C = 0.0134$ and $m = 1$ are the JC constants; and the melting temperature ($T_m$) is 1460 °C for AISI 1045 steel [24]. The shear velocity ($V_s$) is calculated by [9]

$$V_s = \frac{\cos\alpha}{\cos(\phi-\alpha)}V_c. \tag{3}$$

According to Oxley [9], the average temperature due to plastic work in the shear zone can be calculated by

$$T_{AB} = T_r + \eta\,\frac{1-\beta_T}{\rho\,S f\,w}\frac{F_s\cos\alpha}{\cos(\phi-\alpha)}. \tag{4}$$

Xiong et al. [14] informed that the shear zone temperature factor ($\eta$) and the tool/chip interface temperature factor ($\psi$) had an important effect on the estimation accuracy. For calculating the temperature on the shear plane ($T_{AB}$), the factor $\eta$ can be evaluated by comparing the estimated outcomes with the measured cutting force ($F_{ci}$), feed force ($F_{fi}$), average temperature of tool/chip interface ($T_{inti}$) and chip thickness ($t_{ci}$) for index $i = 1, 2, 3 \ldots, N$.

For $\eta = \eta_j$ ($j = 1, 2 \ldots, M$), a quadratic sum of relative errors ($E_j$) of the estimated results ($F_{c,ij}$, $F_{f,ij}$, $T_{int,ij}$ and $t_{c,ij}$) to experimental data are calculated by

$$E_j = \sum_{i=1}^{N}\left[\left(\frac{F_{c,ij}-F_{ci}}{F_{ci}}\right)^2 + \left(\frac{F_{f,ij}-F_{fi}}{F_{fi}}\right)^2 + \left(\frac{T_{int,ij}-T_{inti}}{T_{inti}}\right)^2 + \left(\frac{t_{c,ij}-t_{ci}}{t_{ci}}\right)^2\right]. \tag{5}$$

Assume that

$$E_k = \min(E_j) \text{ then } \eta = \eta_k. \tag{6}$$

The experimental results obtained by Ivester et al. [25] are considered to determine the temperature factor $\eta$. The conditions for orthogonal machining are: AISI 1045 steel as workpiece material; uncoated tungsten carbide/cobalt inserts with rake angle ($\alpha$) −7 and +5°; cutting speed ($V_c$) 200 and 300 m/min, feed rate ($f$) 0.15 and 0.30 mm/rev and width of cut ($w$) 1.6 mm. The thermo-physical properties of the workpiece material are given in Table 1.

**Table 1** Properties of workpiece material [9]

| Density, $\rho$ (kg/m$^3$) | Thermal conductivity, $\lambda_c$ (W/mK) | Specific heat, $S$ (J/kgK) |
|---|---|---|
| 7850 | 52.61–0.0281$T$ | 420 + 0.504$T$ |

Assuming $\eta = 0.5$, 0.6, 0.7, 0.8, 0.9, 1 and considering $\psi = 0.75$ based on Xiong et al.'s study [14], the shear zone temperature factor ($\eta$) is evaluated as 1 with the above method.

### 2.3 Tool–chip interface

A rectangular plastic zone with thickness $\delta\,t_c$ at the tool/chip interface is supposed and the equivalent strain rate is

$$\dot{\varepsilon}_{int} = \frac{\dot{\gamma}_{int}}{\sqrt{3}} = \frac{1}{\sqrt{3}}\frac{V_{ch}}{\delta\,t_c}, \tag{7}$$

where the chip flow velocity ($V_{ch}$) is expressed by:

$$V_{ch} = \frac{\sin\phi}{\cos(\phi-\alpha)}V_c. \tag{8}$$

Material outflow velocities considerably influence the temperature distributions. To account for this effect, the velocity of the chip outflow is defined by

$$V_{ch}(l_i) = \begin{cases} V_{ch}\left(\frac{l_i}{l_p}\right)^{\xi} & \text{for } 0 \le l_i \le l_p \text{ sticking zone,} \\ V_{ch} & \text{for } l_p \le l_i \le l_c \text{ sliding zone.} \end{cases} \tag{9}$$

The equivalent maximum shear strain is expressed by [26]

$$\varepsilon_{int} = \frac{\gamma_{int}}{\sqrt{3}} = \frac{1}{\sqrt{3}}\left(2\gamma_{AB} + \frac{l_c}{2\delta\,t_c}\right). \tag{10}$$

Based on the basic force relations, the components of force are given by

$$\begin{cases} F_c = R\cos(\beta_a-\alpha),\ F_f = R\sin(\beta_a-\alpha),\ F_s = k_{AB}l_{AB}w, \\ F = R\sin\beta_a,\ N = R\cos\beta_a, \\ R = \frac{F_s}{\cos\theta} = \frac{k_{AB}f\,w}{\sin\phi\,\cos\theta}, \end{cases} \tag{11}$$

where $\theta$ is the angle between the resultant force ($R$) and $AB$, the following relationship was derived:

$$\tan\theta = 1 + 2\left(\frac{\pi}{4}-\phi\right) - \left(\frac{dk}{ds_2}\right)_{AB}\frac{l_{AB}}{2k_{AB}}, \tag{12}$$

where $(dk/ds_2)_{AB}$ $(l_{AB}/2k_{AB})$ is expressed by:

$$\left(\frac{dk}{ds_2}\right)_{AB}\frac{l_{AB}}{2k_{AB}} = \left(\frac{1}{3}\frac{d\sigma_{AB}}{d\varepsilon_{AB}}\right)\left(\frac{C_0V_s}{l_{AB}}\right)\left(\frac{1}{V_c\sin\phi}\right)\frac{l_{AB}}{2k_{AB}}, \tag{13}$$

in which $ds_2$ is the thickness of the primary shear zone.

Substituting $V_s/V_c \sin\phi = 2\sqrt{3}\varepsilon_{AB}$ and $k_{AB} = \sigma_{AB}/\sqrt{3}$ in Eq. (13) gives

$$\left(\frac{dk}{ds_2}\right)_{AB} \frac{l_{AB}}{2k_{AB}} = C_0 \left(\frac{d\sigma_{AB}}{d\varepsilon_{AB}}\right)\left(\frac{\varepsilon_{AB}}{\sigma_{AB}}\right), \tag{14}$$

where the term

$$\left(\frac{d\sigma_{AB}}{d\varepsilon_{AB}}\right)\left(\frac{\varepsilon_{AB}}{\sigma_{AB}}\right) \tag{15}$$

is the strain-hardening constant ($n_{eq}$).

Substituting Eq. (14) into Eq. (12), the following relationship can be obtained:

$$\tan\theta = 1 + 2\left(\frac{\pi}{4} - \phi\right) - C_0 n_{eq}. \tag{16}$$

For the JC material model, $d\sigma_{AB}/d\varepsilon_{AB}$ can be written as

$$\frac{d\sigma_{AB}}{d\varepsilon_{AB}} = nB\varepsilon_{AB}^{n-1}\left(1 + C\,\mathrm{In}\frac{\dot{\varepsilon}_{AB}}{\dot{\varepsilon}_0}\right)(1 - T_{AB}^{*m}) + (A + B\varepsilon_{AB}^{n})\left(1 + C\,\mathrm{In}\frac{\dot{\varepsilon}_{AB}}{\dot{\varepsilon}_0}\right)\left(\frac{-m}{(T_{AB} - T_r)}\right)T_{AB}^{*m}\left(\frac{\beta_T\,\sigma_{AB}}{\rho\,S}\right), \tag{17}$$

where $T_{AB}^{*m} = (T_{AB} - T_r)/(T_m - T_r)$.

Substituting Eq. (17) into Eq. (15), the strain-hardening constant ($n_{eq}$) becomes

$$n_{eq} = \left[\frac{nB\varepsilon_{AB}^{n}}{(A + B\varepsilon_{AB}^{n})} - \varepsilon_{AB}\left(\frac{m}{(T_{AB} - T_r)}\right)\left(\frac{T_{AB}^{*m}}{1 - T_{AB}^{*m}}\right)\left(\frac{\beta_T\,\sigma_{AB}}{\rho\,S}\right)\right]. \tag{18}$$

Because of $1/\rho\,S \cong 0$, the strain-hardening constant ($n_{eq}$) can be finally determined through the above approach proposed by Lalwani et al. [13] as follows:

$$n_{eq} \approx \frac{nB\varepsilon_{AB}^{n}}{(A + B\varepsilon_{AB}^{n})}. \tag{19}$$

The shear flow stress in the chip is found using

$$k_{chip} = \frac{1}{\sqrt{3}}(A + B\varepsilon_{int}^{n})\left(1 + C\,\mathrm{In}\frac{\dot{\varepsilon}_{int}}{\dot{\varepsilon}_0}\right)\left(1 - \left(\frac{T_{int} - T_r}{T_m - T_r}\right)^{m}\right). \tag{20}$$

Supposing the uniform normal stress at the tool/chip interface, $\sigma_N$ and $\tau_{int}$ are expressed as $\sigma_N = \frac{N}{l_c w}$,

$$\tau_{int} = \frac{F}{l_c w}, \tag{21}$$

where the tool/chip contact length ($l_c$) is calculated by:

$$l_c = \frac{f\sin\theta}{\cos\beta_a \sin\phi}\left(1 + \frac{C_0\,n_{eq}}{3\left[1 + 2\left(\frac{\pi}{4} - \phi\right) - C_0\,n_{eq}\right]}\right). \tag{22}$$

Temperature variation over the rake face is dependent on normal and frictional stress distributions. To obtain non-uniform heat partition along the tool/chip interface, the stress distribution is described by non-uniform distributions [23].

The normal stress distribution ($\sigma_N(l_i)$) over the rake face is calculated by [27, 28]

$$\sigma_N(l_i) = \sigma_N'\left(1 - \frac{l_i}{l_c}\right)^{\xi}, \tag{23}$$

where the $\sigma_N'$ is determined by:

$$\sigma_N' = k_{AB}\left(1 + \frac{\pi}{2} - 2\alpha - 2C_0 n_{eq}\right). \tag{24}$$

To evaluate the variation of the shear stress ($\tau_{int}(l_i)$), the following relationship is used [27, 29]:

$$\tau_{int}(l_i) = \begin{cases} \tau_{st}(l_i) & \text{for } 0 \le l_i \le l_p \text{ sticking,} \\ \mu_{local}\,\sigma_N'\left(1 - \frac{l_i}{l_c}\right)^{\xi} & \text{for } l_p \le l_i \le l_c \text{ sliding.} \end{cases} \tag{25}$$

Using the global friction angle ($\beta_a = \arctan(\mu)$), the local friction coefficient ($\mu_{local}$) is calculated by

$$\mu_{local} = \frac{l_c^{\xi+1}\,\tan\beta_a}{(l_p\xi + l_c)(l_c - l_p)^{\xi}}. \tag{26}$$

The average interface temperature is given by

$$T_{int} = T_{AB} + \psi\,\Delta T_{M,c}. \tag{27}$$

The value of $\psi$ is found as 0.75 for AISI 1045 steel, comparing estimated results to measured values through the one which is similar to the method proposed for the shear zone temperature factor $\eta$ [14].

Finally, Boothroyd [30] presented the following equation to evaluate the maximum temperature increase in the chip ($\Delta T_{M,c}$):

$$\log\left(\frac{\Delta T_{M,c}}{\Delta T_c}\right) = 0.06 - 0.195\delta\sqrt{\frac{R_T\,t_c}{l_c}} + 0.5\log\left(\frac{R_T\,t_c}{l_c}\right). \tag{28}$$

## 3 Thermal modeling of metal cutting

### 3.1 Primary heat source

Komanduri and Hou [16] enabled a heat source model to evaluate the temperature distribution in the primary deformation zone. This model considers the workpiece and chip, as schematically illustrated in Fig. 2. The shear plane is depicted as the band heat source with the intensity of $q_{shear}$ acting obliquely at an angle $\varphi$ with a velocity $V$ in a semi-infinite medium. The uncut surface of the workpiece and the upper surface of the chip are adiabatic. An imaginary heat source is incorporated into the model.

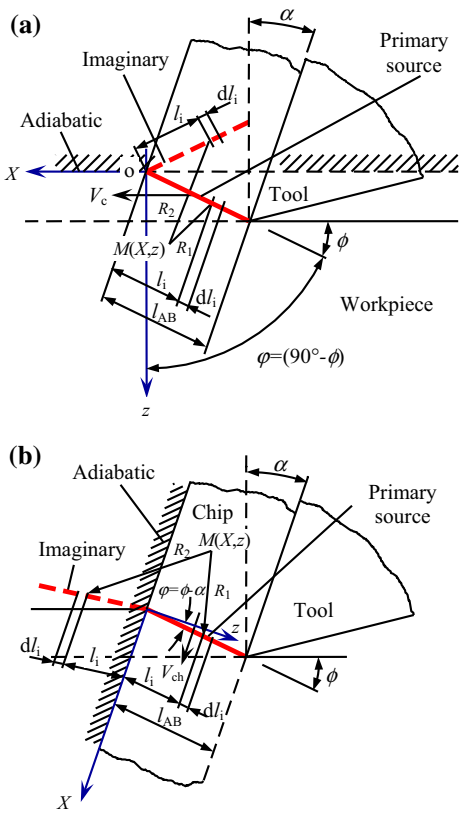


**Fig. 2** Thermal modeling of primary heat source: **a** workpiece, **b** chip [16]

The temperature increase at a point $M(X,z)$ is expressed by

$$T_{\mathrm{M}} = \frac{q_{\mathrm{shear}}}{2\pi\lambda_{\mathrm{c}}} \int_0^{l_{\mathrm{AB}}} \mathrm{e}^{-(X-l_{\mathrm{i}}\sin\varphi)\,V/2a} \times \left\{ K_0\left[\frac{V}{2a}\sqrt{(X-l_{\mathrm{i}}\sin\varphi)^2+(z-l_{\mathrm{i}}\cos\varphi)^2}\right] + K_0\left[\frac{V}{2a}\sqrt{(X-l_{\mathrm{i}}\sin\varphi)^2+(z+l_{\mathrm{i}}\cos\varphi)^2}\right] \right\} \mathrm{d}l_{\mathrm{i}}. \tag{29}$$

The heat intensity ($q_{\mathrm{shear}}$) due to shearing can be uniformly expressed by

$$q_{\mathrm{shear}} = k_{\mathrm{AB}}\, V_{\mathrm{s}}. \tag{30}$$

$V$ and $\varphi$ depend on the thermal effect of the primary deformation zone, namely $V = V_{\mathrm{c}}$ and $\varphi = (90^\circ - \phi)$ for the workpiece and $V = V_{\mathrm{ch}}$ and $\varphi = (\phi - \alpha)$ for the chip.

### 3.2 Secondary heat source

Taking into by consideration a non-uniform distribution of the heat partition ratio within a semi-infinite medium, the solutions for thermal analysis of the chip and tool were presented in Komanduri and Hou's study [17]. Figure 3a shows the thermal analysis model of the chip. A band acting with a velocity $V_{\mathrm{ch}}$ is described as the secondary heat source. The tool/chip interface and the upper surface of the chip are adiabatic. Taking into consideration the heat partition ratio function $B_{\mathrm{i,chip}}$ for the chip, the heat liberation ratio of the acting band heat source is obtained to be $B_{\mathrm{i,chip}}\, q_{\mathrm{friction}}$.

The temperature increase of each point of the chip is expressed by

$$T_{\mathrm{M}} = \frac{1}{\pi\lambda_{\mathrm{c}}} \int_0^{l_{\mathrm{c}}} B_{\mathrm{i,chip}}\, q_{\mathrm{friction}}\, e^{-(X-l_{\mathrm{i}})\,V_{\mathrm{ch}}/2a} \times [K_0(R_1 V_{\mathrm{ch}}/2a) + K_0(R_2 V_{\mathrm{ch}}/2a)]\, \mathrm{d}l_{\mathrm{i}}, \tag{31}$$

where $R_1 = \sqrt{(X-l_{\mathrm{i}})^2 + z^2}$ and $R_2 = \sqrt{(X-l_{\mathrm{i}})^2 + (2t_{\mathrm{c}} - z)^2}$.

The nonlinear heat intensity can be determined by

$$q_{\mathrm{friction}} = \tau_{\mathrm{int}}(l_{\mathrm{i}})\, V_{\mathrm{ch}}(l_{\mathrm{i}}). \tag{32}$$

Figure 3b illustrates the thermal analysis model for the tool. A stationary rectangular plane is depicted as the secondary heat source. The clearance face is adiabatic. Taking into consideration the heat partition ratio function $B_{\mathrm{i,tool}}$ for

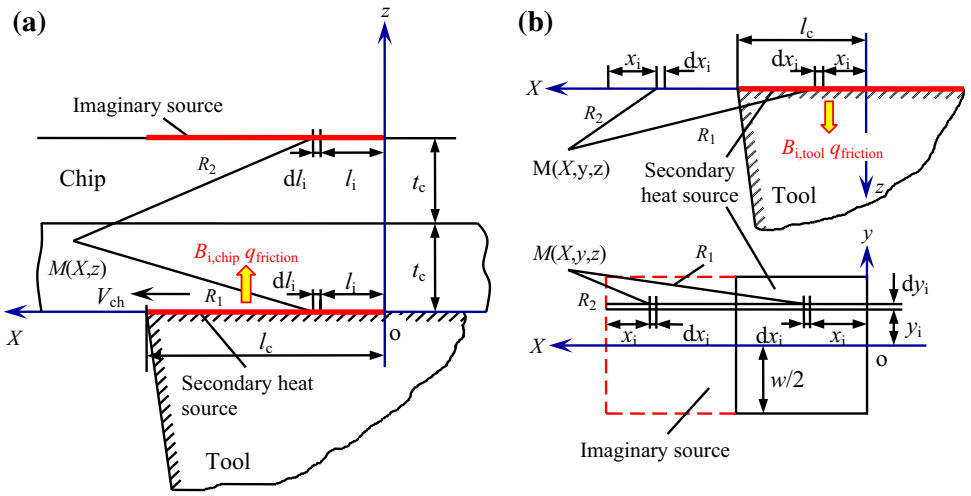


**Fig. 3** Thermal modeling of secondary heat source: **a** chip; **b** tool [17]

the tool, the heat liberation ratio of the stationary rectangular heat source is obtained to be $B_{\text{i,tool}}\, q_{\text{friction}}$. The temperature increase at a point $M(X, y, z)$ of the tool is calculated by:

$$T_{\text{M}} = \frac{1}{2\pi\lambda_{\text{t}}} \int_0^{l_{\text{c}}} B_{\text{i,tool}}\, q_{\text{friction}} \mathrm{d}x_{\text{i}} \int_{-w/2}^{w/2} \left(\frac{1}{R_1} + \frac{1}{R_2}\right) \mathrm{d}y_{\text{i}}, \tag{33}$$

where $R_1 = \sqrt{(X - x_{\text{i}})^2 + (y - y_{\text{i}})^2 + z^2}$ and $R_2 = \sqrt{(X - 2l_{\text{c}} + x_{\text{i}})^2 + (y - y_{\text{i}})^2 + z^2}$.

The intensities of the acting and stationary heat sources are non-uniformly distributed. To obtain a satisfactory solution for the acting band and stationary heat sources having variable heat intensity, the following heat partition equations given in Ref. [17] are substituted into Eqs. (31) and (33).

$$B_{\text{i, chip}} = (0.620 - 0.35) + 2 \times 0.35 \left(\frac{l_{\text{i}}}{l_{\text{c}}}\right)^{0.24} + 2 \times 0.35 \left(\frac{l_{\text{i}}}{l_{\text{c}}}\right)^{16} \tag{34}$$

$$B_{\text{i, tool}} = (0.380 + 0.35) - 2 \times 0.35 \left(\frac{l_{\text{i}}}{l_{\text{c}}}\right)^{0.24} - 2 \times 0.35 \left(\frac{l_{\text{i}}}{l_{\text{c}}}\right)^{16} \tag{35}$$

### 3.3 United influence of heat sources

The temperature increase in metal cutting depends on their united influences of primary and secondary heat sources [18]. The temperature increase on the chip can be described by taking into consideration the primary heat source as a uniform acting oblique band and the secondary heat source as a non-uniform acting band with their imaginaries in a semi-infinite medium.

The temperature increase at a point $M(X, z)$ of the chip is determined by summing the united influences of two principle heat sources which are given by Eqs. (29) and (31)

$$\begin{aligned} T_{\text{M}} = {} & \frac{q_{\text{shear}}}{2\pi\lambda_{\text{c}}} \int_0^{t_{\text{c}}/\cos(\phi-\alpha)} \mathrm{e}^{-(X-X_{\text{i}})\, V_{\text{ch}}/2a} \\ & \times \left\{ K_0 \left[ \frac{V_{\text{ch}}}{2a} \sqrt{(X - X_{\text{i}})^2 + (z - z_{\text{i}})^2} \right] \right. \\ & \left. + K_0 \left[ \frac{V_{\text{ch}}}{2a} \sqrt{(X - X_{\text{i}})^2 + (2t_{\text{c}} - z - z_{\text{i}})^2} \right] \right\} \mathrm{d}w_{\text{i}} \\ & + \frac{1}{\pi\lambda_{\text{c}}} \int_0^{l_{\text{c}}} B_{\text{i,chip}}\, q_{\text{friction}}\, e^{-(X-l_{\text{i}})\, V_{\text{ch}}/2a} \\ & \times [K_0(R_1 V_{\text{ch}}/2a) + K_0(R_2 V_{\text{ch}}/2a)]\, \mathrm{d}l_{\text{i}}, \end{aligned} \tag{36}$$

where $X_{\text{i}} = l_{\text{c}} - w_{\text{i}} \sin(\phi - \alpha)$ and $z_{\text{i}} = w_{\text{i}} \cos(\phi - \alpha)$.

The temperature increase of the tool is expressed by modeling the secondary heat source as a non-uniform stationary rectangular heat source. The primary heat source indirectly contributes as an induced heat source to the temperature increase on the tool. Equation (33) is used to calculate the average intensity of the induced heat source ($q_{\text{induced}}$). Considering the induced heat liberation ratio of the primary heat source ($B'_{\text{i,tool}}\, q_{\text{induced}}$), the heat is entirely conducted into the tool. Thus, the temperature increase of each point of the tool is expressed as

$$\begin{aligned} T_{\text{M}} = {} & \frac{1}{2\pi\lambda_{\text{t}}} \int_0^{l_{\text{c}}} B_{\text{i,tool}}\, q_{\text{friction}}\, \mathrm{d}x_{\text{i}} \int_{-w/2}^{w/2} \left(\frac{1}{R_1} + \frac{1}{R_2}\right) \mathrm{d}y_{\text{i}} \\ & + \frac{1}{2\pi\lambda_{\text{t}}} \int_0^{l_{\text{c}}} B'_{\text{i,tool}}\, q_{\text{induced}}\, \mathrm{d}x_{\text{i}} \int_{-w/2}^{w/2} \left(\frac{1}{R_1} + \frac{1}{R_2}\right) \mathrm{d}y_{\text{i}}, \end{aligned} \tag{37}$$

where $R_1 = \sqrt{(X - x_{\text{i}})^2 + (y - y_{\text{i}})^2 + z^2}$, $R_2 = \sqrt{(X - 2l_{\text{c}} + x_{\text{i}})^2 + (y - y_{\text{i}})^2 + z^2}$ and $x_{\text{i}} = l_{\text{i}}$. The heat partition ratio ($B'_{\text{i, tool}}$) is evaluated by [18]

$$B'_{\text{i, tool}} = (1 + 0.8) - 2 \times 0.8 \left(\frac{x_{\text{i}}}{l_{\text{c}}}\right)^{0.3} - 0.2 \times 0.8 \left(\frac{x_{\text{i}}}{l_{\text{c}}}\right)^{4}. \tag{38}$$

## 4 Results and discussion

### 4.1 The results of the improved Oxley's model

For the improved Oxley's model, the properties of the workpiece material and cutting parameters were input variables. On the other hand, the output ones were results such as shear angle, chip thickness, force and stress. Table 2 shows the estimated process information from the improved Oxley's model in machining conditions of Ref. [25]. In this table, cutting forces $F_{\text{c,E}}$ and $F_{\text{c,I}}$, feed forces $F_{\text{f,E}}$ and $F_{\text{f,I}}$ and chip thicknesses $t_{\text{c,E}}$ and $t_{\text{c,I}}$ calculated with the extended model by Lalwani et al. [13] and the improved model as well as their relative differences $\Delta F_{\text{c}}$, $\Delta F_{\text{f}}$ and $\Delta t_{\text{c}}$ were listed. The results showed that the maximum relative differences of $F_{\text{c}}$, $F_{\text{f}}$ and $t_{\text{c}}$, were 17.4, 61.3 and 29.4 %, respectively.

To study the influence of the improved Oxley's model on the estimation accuracy, the process results calculated using the improved Oxley's model and the estimation outcomes of Lalwani et al.'s extended model [13] were compared with measurement results given in Ref. [25] for AISI 1045 steel. Figures 4, 5 and 6 illustrate comparisons of the cutting force ($F_{\text{c}}$), feed force ($F_{\text{f}}$) and chip thickness ($t_{\text{c}}$). It was found from Fig. 4 that the absolute percentage errors ($\varepsilon_{\text{I}}$) between the cutting forces ($F_{\text{c}}$) measured and estimated from the improved model for tool with negative rake angle were lesser than 8 %. The highest absolute percentage error ($\varepsilon_{\text{E}}$) between the $F_{\text{c}}$ values measured and obtained from the extended model by Lalwani et al. [13] for tool with negative rake angle was as high as about 15 %. For tool with positive rake angle, the errors of the $F_{\text{c}}$ values estimated from the improved model were approximately within 13–20 %

**Table 2** Calculated results from the extended Oxley's model by Lalwani et al. [13] and improved Oxley's model in this study

| Test | 1 | 2 | 3 | 4 | 5 | 6 | 7 | 8 |
|---|---|---|---|---|---|---|---|---|
| $V_c$ (m/min) | 200 | | | | 300 | | | |
| $f$ (mm/rev) | 0.15 | | 0.30 | | 0.15 | | 0.30 | |
| $\alpha$ (°) | −7 | 5 | −7 | 5 | −7 | 5 | −7 | 5 |
| $\delta$ | 0.0504 | 0.0604 | 0.0304 | 0.0304 | 0.0404 | 0.4040 | 0.0244 | 0.0204 |
| $C_0$ | 6.0060 | 4.5540 | 5.7070 | 4.0380 | 5.8240 | 4.2310 | 5.5470 | 3.7530 |
| $\phi$ | 16.404 | 24.796 | 19.532 | 28.432 | 18.294 | 27.062 | 21.306 | 30.506 |
| $\varepsilon_{AB}$ | 1.1055 | 0.7287 | 0.9578 | 0.6582 | 1.0096 | 0.6820 | 0.8956 | 0.6276 |
| $\dot{\varepsilon}_{AB}$ ($s^{-1}$) | 23,536 | 25,944 | 13,579 | 13,391 | 38,623 | 39,820 | 21,864 | 20,234 |
| $\varepsilon_{int}$ | 8.8369 | 6.5801 | 12.517 | 10.958 | 10.102 | 8.7604 | 14.776 | 15.241 |
| $\dot{\varepsilon}_{int}$ ($s^{-1}$) | 24,106 | 42,202 | 29,467 | 56,820 | 57,417 | 114,790 | 67,167 | 149,220 |
| $T_{AB}$ (°C) | 407.39 | 313.12 | 383.10 | 300.77 | 393.31 | 306.30 | 374.64 | 297.80 |
| $T_{int}$ (°C) | 895.07 | 815.74 | 992.44 | 941.15 | 947.81 | 891.20 | 1049.8 | 1018.0 |
| $n_{eq}$ | 0.1232 | 0.1175 | 0.1212 | 0.1161 | 0.1219 | 0.1166 | 0.1203 | 0.1154 |
| $\theta$ (°) | 51.523 | 49.482 | 50.125 | 47.970 | 50.703 | 48.563 | 49.227 | 47.006 |
| $F_{c,I}$ (N) | 625.42 | 464.69 | 1077.7 | 816.02 | 574.55 | 431.67 | 1003.6 | 766.03 |
| $F_{c,E}$ (N) | 576 | 433 | 1007 | 773 | 533 | 406 | 1041 | 899 |
| $\Delta F_c$ (%) | −7.9 | −6.8 | −6.6 | −5.3 | −7.2 | −5.9 | 3.7 | 17.4 |
| $F_{f,I}$ (N) | 439.86 | 213.60 | 637.19 | 289.58 | 364.74 | 170.05 | 531.84 | 226.91 |
| $F_{f,E}$ (N) | 364 | 171 | 533 | 233 | 302 | 136 | 550 | 366 |
| $\Delta F_f$ (%) | −17.2 | −19.9 | −16.4 | −19.5 | −17.2 | −20.0 | 3.4 | 61.3 |
| $t_{c,I}$ (mm) | 0.48745 | 0.33653 | 0.80281 | 0.57814 | 0.43206 | 0.30556 | 0.72693 | 0.53339 |
| $t_{c,E}$ (mm) | 0.43 | 0.31 | 0.72 | 0.54 | 0.38 | 0.28 | 0.79 | 0.69 |
| $\Delta t_c$ (%) | −11.8 | −7.9 | −10.3 | −6.6 | −12.0 | −8.4 | 8.7 | 29.4 |
| $V_{ch}$ (m/s) | 1.0258 | 1.4858 | 1.2456 | 1.7297 | 1.7359 | 2.4545 | 2.0635 | 2.8122 |
| $l_c$ (mm) | 0.56388 | 0.36069 | 0.89624 | 0.58698 | 0.48875 | 0.31629 | 0.79783 | 0.52715 |
| $k_{AB}$ (MPa) | 559.81 | 580.63 | 559.09 | 575.03 | 563.73 | 582.05 | 561.49 | 576.16 |
| $\tau_{int}$ (MPa) | 399.43 | 438.90 | 349.44 | 382.89 | 373.41 | 409.09 | 317.71 | 347.16 |
| $k_{chip}$ (MPa) | 399.44 | 438.85 | 349.49 | 382.89 | 373.35 | 409.05 | 317.72 | 347.17 |
| $\sigma'_N$ (MPa) | 747.45 | 769.91 | 800.18 | 838.69 | 786.10 | 820.44 | 831.12 | 881.30 |
| $\sigma_N$ (MPa) | 747.46 | 769.90 | 800.12 | 838.69 | 786.09 | 820.46 | 831.09 | 881.31 |

$\Delta F_c = \frac{F_{c,E}-F_{c,I}}{F_{c,I}} 100\ \%, \Delta F_f = \frac{F_{f,E}-F_{f,I}}{F_{f,I}} 100\ \%$ and $\Delta t_c = \frac{t_{c,E}-t_{c,I}}{t_{c,I}} 100\ \%$

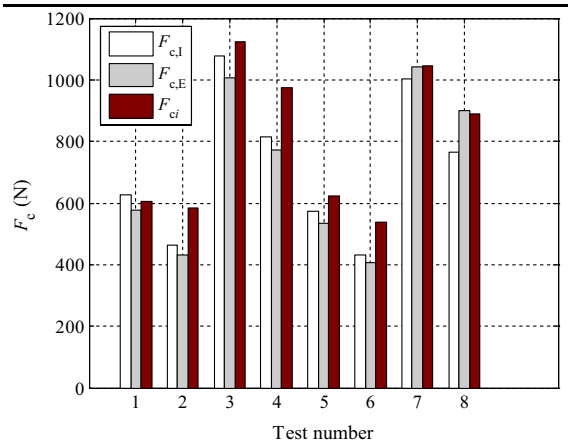


| Test number | $\alpha$ (°) | $F_{c,I}$ (N) | $F_{c,E}$ (N) | $F_{ci}$ (N) | $\varepsilon_I$ (%) | $\varepsilon_E$ (%) |
|---|---|---|---|---|---|---|
| 1 | -7 | 625.42 | 576 | 607 | 3.03 | 5.11 |
| 2 | 5 | 464.69 | 433 | 583 | 20.29 | 25.73 |
| 3 | -7 | 1077.7 | 1007 | 1125 | 4.20 | 10.49 |
| 4 | 5 | 816.02 | 773 | 976 | 16.39 | 20.80 |
| 5 | -7 | 574.55 | 533 | 623 | 7.78 | 14.45 |
| 6 | 5 | 431.67 | 406 | 539 | 19.91 | 24.68 |
| 7 | -7 | 1003.6 | 1041 | 1045 | 3.96 | 0.38 |
| 8 | 5 | 766.03 | 899 | 888 | 13.74 | 1.24 |

**Fig. 4** Comparison of the cutting forces calculated from the extended and improved Oxley's models with the measured ones

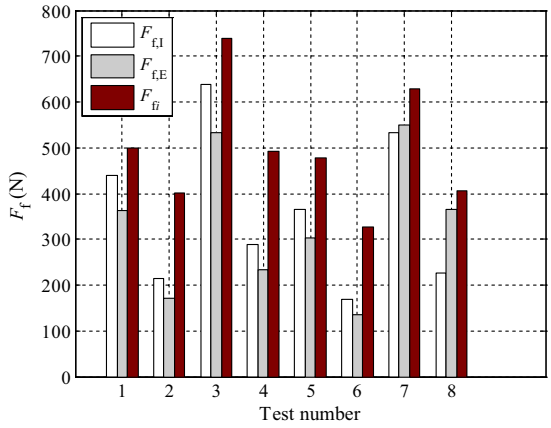


| Test number | $\alpha$ (°) | $F_{f,I}$ (N) | $F_{f,E}$ (N) | $F_{fi}$ (N) | $\varepsilon_I$ (%) | $\varepsilon_E$ (%) |
|---|---|---|---|---|---|---|
| 1 | -7 | 439.86 | 364 | 500 | 12.03 | 27.20 |
| 2 | 5 | 213.6 | 171 | 402 | 46.87 | 57.46 |
| 3 | -7 | 637.19 | 533 | 740 | 13.89 | 27.97 |
| 4 | 5 | 289.58 | 233 | 493 | 41.26 | 52.74 |
| 5 | -7 | 364.74 | 302 | 478 | 23.69 | 36.82 |
| 6 | 5 | 170.05 | 136 | 326 | 47.84 | 58.28 |
| 7 | -7 | 531.84 | 550 | 628 | 15.31 | 12.42 |
| 8 | 5 | 226.91 | 366 | 406 | 44.11 | 9.85 |

**Fig. 5** Comparison of the feed forces calculated from the extended and improved Oxley's models with the measured ones

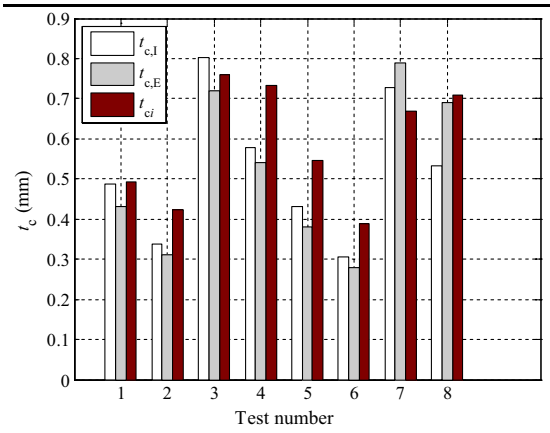


| Test number | $\alpha$ (°) | $t_{c,I}$ (N) | $t_{c,E}$ (N) | $t_{ci}$ (N) | $\varepsilon_I$ (%) | $\varepsilon_E$ (%) |
|---|---|---|---|---|---|---|
| 1 | -7 | 0.48745 | 0.43 | 0.493 | 1.13 | 12.78 |
| 2 | 5 | 0.33653 | 0.31 | 0.424 | 20.63 | 26.89 |
| 3 | -7 | 0.80281 | 0.72 | 0.759 | 5.77 | 5.14 |
| 4 | 5 | 0.57814 | 0.54 | 0.734 | 21.23 | 26.43 |
| 5 | -7 | 0.43206 | 0.38 | 0.546 | 20.87 | 30.40 |
| 6 | 5 | 0.30556 | 0.28 | 0.389 | 21.45 | 28.02 |
| 7 | -7 | 0.72693 | 0.79 | 0.668 | 8.82 | 18.26 |
| 8 | 5 | 0.53339 | 0.69 | 0.709 | 24.77 | 2.68 |

**Fig. 6** Comparison of the chip thicknesses calculated from the extended and improved Oxley's models with the measured ones

range. This range is acceptable for practical purpose. The $F_c$ values of Lalwani et al. [13] had more percentage error than 20 % for tool with positive rake angle, except for test 8 with cutting speed $V_c = 300$ m/min, feed rate $f = 0.3$ mm/rev and rake angle $\alpha = 5°$.

For tool with negative rake angle as illustrated in Fig. 5, the errors ($\varepsilon_I$) between the feed forces ($F_f$) measured and estimated from the improved model were obtained at lesser than 16 %, except for test 5 with cutting speed $V_c = 300$ m/min, feed rate $f = 0.15$ mm/rev and rake angle $\alpha = -7°$. The greatest percentage error ($\varepsilon_E$) between the $F_f$ values measured and obtained from Lalwani et al.'s extended model [13] for tool with negative rake angle reached up to about 36 %. For tool with positive rake angle, the estimated feed forces from the improved model were found to be more accurate than the estimation results of Lalwani et al. [13].

From the results given in Fig. 6, the absolute percentage errors ($\varepsilon_I$) between the chip thicknesses ($t_c$) measured and obtained from the improved model were found as lesser than 9 % for tool with negative rake angle, except for test 5 with cutting speed $V_c = 300$ m/min, feed rate $f = 0.15$ mm/rev and rake angle $\alpha = -7°$. The greatest percentage error ($\varepsilon_E$) between the experimental data and the results of Lalwani et al. [13] was approximately 30 % for tool with negative rake angle. For tool with positive rake angle, the estimated outcomes $t_c$ from the improved model showed a good agreement with the experimental values. The percentage errors between the $t_c$ values of Lalwani et al. [13] and the experimental results for tool with positive rake angle were mostly greater than those of the improved model.

Consequently, the results of $F_c$, $F_f$ and $t_c$ estimated with the improved model were closer to the experimental values than the estimation outcomes of Lalwani et al.

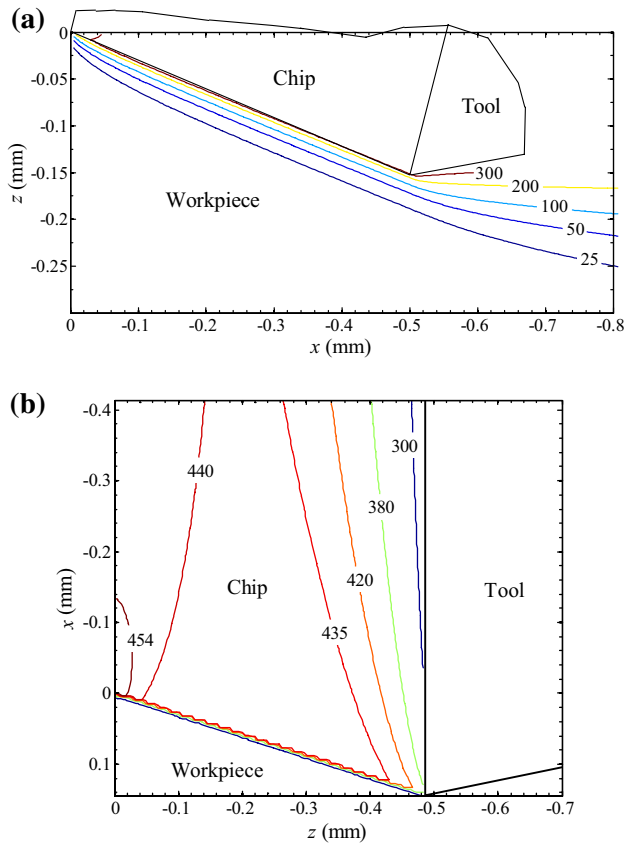


**Fig. 7** Temperature maps due to primary heat source for test 1 ($V_c = 200$ m/min, $f = 0.15$ mm/rev, $w = 1.6$ mm, $\alpha = -7°$): **a** workpiece; **b** chip

[13]. Therefore, it was concluded that the presented model resulted in higher accuracy of the $F_c$, $F_f$ and $t_c$ values due to improvements in shear zone and interface temperature factors.

### 4.2 Temperature distributions in chip and workpiece due to a primary heat source

To compute temperature distributions in machining of AISI 1045 steel, input variables, namely shear angle ($\phi$), shear force ($F_s$), shear velocity ($V_s$), shear plane length ($l_{AB}$), chip velocity ($V_{ch}$) and shear heat source intensity ($q_{shear}$), have been calculated by considering the improved Oxley's theory. The properties of the workpiece were evaluated as temperature dependent. The thermal conductivity of the tool was taken as 100 W/(mK).

Figure 7 shows the maps of the temperature distributions within the workpiece and chip generated by the primary heat source. As observed from Fig. 7a, the temperature distribution of the workpiece was concentrated around the primary shear zone because of excessive plastic deformation of the workpiece material to generate the chip. The highest workpiece temperature around the shear plane due to the primary heat source acting with the velocity $V_c$ at the angle $\varphi = (90° - \phi)$ was 300 °C. In Fig. 7b, a considerable difference in the temperature increase on both sides of the primary heat source was observed, i.e., the highest chip temperature in the vicinity of the shear plane due to the primary heat source acting with the velocity $V_{ch}$ at the angle $\varphi = (\phi - \alpha)$ was changed to about 450 °C. This temperature difference can be associated with the shear plane depicted through a line in place of the shear zone.

To establish the influence of the cutting conditions on the average chip temperature increase ($\Delta T_c$) generated by the primary heat source only, the temperature values in the chip around the shear plane were also investigated. As shown in Table 3, at the same cutting speed and feed rate, the average temperature increases that occurred in the chip around the primary heat source by using a tool with negative rake angle ($\Delta T_{c,n}$) were greater than the average temperature increases obtained for a tool with positive rake angle ($\Delta T_{c,p}$). The mean difference between $\Delta T_{c,n}$ and $\Delta T_{c,p}$ was also as high as 30.5 %. It was deduced that lower temperatures were generated in the chip around the shear plane by using a tool with positive rake angle. As seen in this table, the temperature values were also sensitive to the increase of the cutting speed. The average temperature values decreased with an increase in cutting speed. For instance, the estimated temperature was 438.1 °C at the cutting speed $V_c = 200$ m/min (test 1) and found as 411.6 °C at the cutting speed $V_c = 300$ m/min (test 5). Such a result was also observed for other tests.

**Table 3** The average temperature increases of the chip around the shear plane

| Test | $V_c$ (m/min) | $f$ (mm/rev) | $\alpha$ (°) | $\Delta T_{c,n}$ (°C) | Test | $V_c$ (m/min) | $f$ (mm/rev) | $\alpha$ (°) | $\Delta T_{c,p}$ (°C) | $\varepsilon T_c$ (%) |
|---|---|---|---|---|---|---|---|---|---|---|
| 1 | 200 | 0.15 | −7 | 438.1 | 2 | 200 | 0.15 | 5 | 329.5 | 33.0 |
| 3 | 200 | 0.30 | −7 | 393 | 4 | 200 | 0.30 | 5 | 302.8 | 29.8 |
| 5 | 300 | 0.15 | −7 | 411.6 | 6 | 300 | 0.15 | 5 | 314 | 31.1 |
| 7 | 300 | 0.30 | −7 | 374.7 | 8 | 300 | 0.30 | 5 | 292.3 | 28.2 |
| Mean difference | | | | | | | | | | 30.5 |

$\varepsilon T_c = \frac{\Delta T_{c-n} - \Delta T_{c-p}}{\Delta T_{c-p}} 100\,\%$

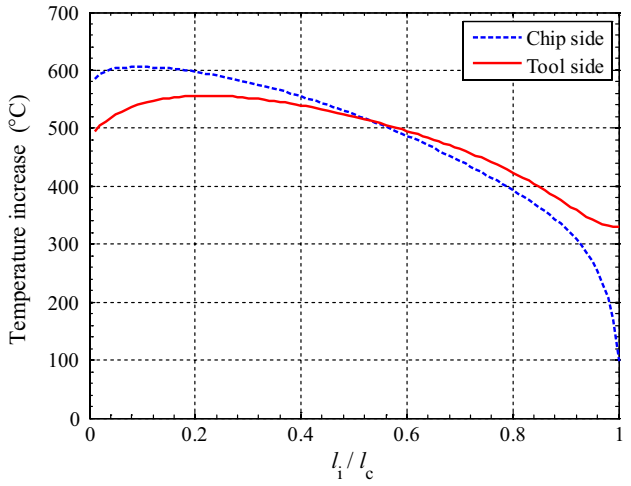


**Fig. 8** Temperature distributions at tool/chip interface due to secondary heat source for test 1 ($V_c = 200$ m/min, $f = 0.15$ mm/rev, $w = 1.6$ mm, $\alpha = -7°$)

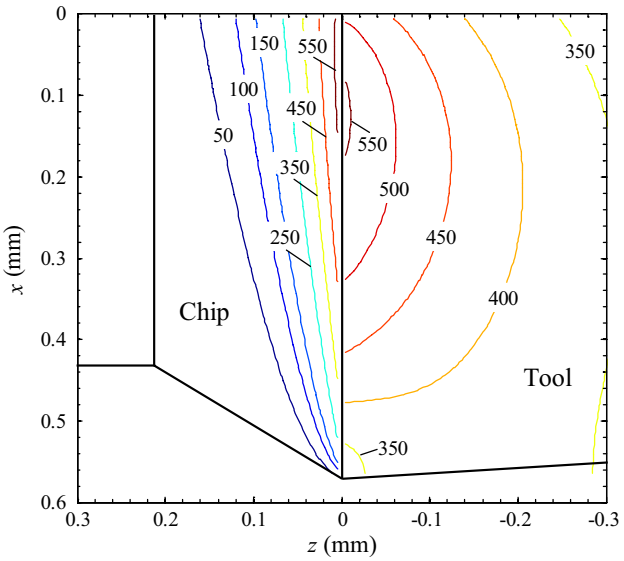


**Fig. 9** Temperature maps of chip and tool caused by secondary heat source for test 1 ($V_c = 200$ m/min, $f = 0.15$ mm/rev, $w = 1.6$ mm, $\alpha = -7°$)

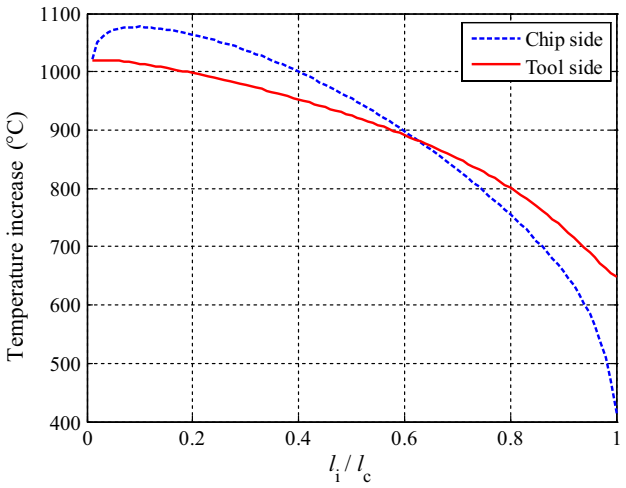


**Fig. 10** Temperature distributions due to the united influence of heat sources for test 1 ($V_c = 200$ m/min, $f = 0.15$ mm/rev, $w = 1.6$ mm, $\alpha = -7°$)

As can be observed from Table 3, the average temperature values indicated a decreasing tendency with an increase of the feed rate at the same cutting speed. The estimated temperature increase was 438.1 °C at the feed rate $f = 0.15$ mm/rev with the cutting speed $V_c = 200$ m/min in test 1. At the feed rate $f = 0.30$ mm/rev with the cutting speed $V_c = 200$ m/min in test 3, the temperature increase was obtained as 393 °C. There was also a similar relationship among other tests.

### 4.3 Temperature distributions of chip and tool due to a secondary heat source

Using Eqs. (31) and (33) and considering the non-uniform heat partition functions for the chip and tool sides, the temperature distributions computed on both sides are illustrated in Fig. 8. It was found that the temperature distribution curves of the chip and tool sides did not exactly match along the contact length due to the difference between the variations of the temperature increase generated by the acting chip and stationary tool. The temperature gradient distribution of the chip side was steeper than that of the tool side. In other words, the tool temperature distribution was more uniform than the other. The heat intensity at the origin ($l_i/l_c = 0$) of the chip was higher than that at the origin of the tool. This result shows that the temperature in the secondary shear zone is affected by heat loss through conduction and the tool temperature is decreased by heat loss. At the other end ($l_i/l_c = 1$), the heat intensity of the chip was lower than that of the tool. The maximum temperature for both sides was obtained to be close to the end of the tool/chip interface. Karpat and Özel [19] also studied the influence of the secondary heat source by implementing a non-uniform heat intensity and found the maximum temperature at some distance back from the tool tip for chip and tool sides.

Figure 9 illustrates the maps of the temperature distributions in the chip and tool generated by the secondary heat source. It was observed that temperature values on both sides gradually increased toward the end of the tool/chip contact zone. In the tool tip vicinity, the tool temperature was found to be about 350 °C, while the chip temperature was approximately in the 50–250 °C range. This is because the acting chip does not experience high contact temperatures for an adequate time.

### 4.4 Temperature distributions due to the united influence of primary and secondary heat sources

Using Eqs. (36) and (37), the temperature distributions at the tool/chip interface caused by the united influence of the primary and secondary heat sources were computed and illustrated in Fig. 10. Based on the estimation results acquired using the improved Oxley's model, the temperature distributions on the chip and tool sides at the tool/chip interface generated by the two heat sources were found to be matched with a satisfactory accuracy. Similarly to the influence of the secondary heat source, the maximum temperature at the tool/chip interface was farther away from the cutting edge. The slope of the temperature distribution curves was toward the cutting edge. The temperature increase gradient near the primary deformation zone was quite steep.

The maps of the temperature distributions in the chip and tool generated by the united influence of the two principal heat sources in machining of AISI 1045 steel are illustrated in Fig. 11. Comparing Figs. 7, 9 and 11, it was inferred that the secondary heat source significantly affected the temperature increase at the tool/chip interface. In other words, the contribution of primary heat source on the temperature increase was less than that of the secondary heat source. This result shows that high cutting speeds cause a flow zone at the interface, and the shear strain in the flow zone is significantly greater than the strain on the shear plane.

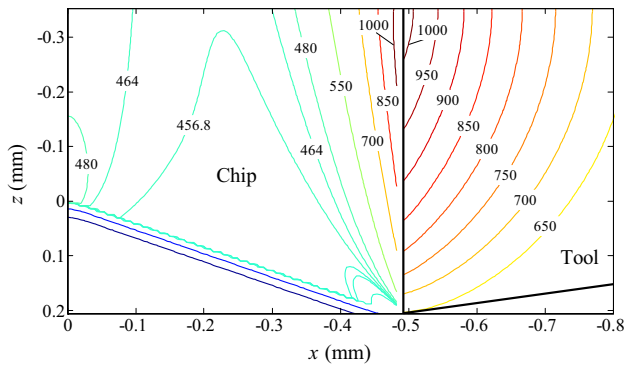


**Fig. 11** Temperature maps in chip and tool considering the united influence of heat sources for test 1 ($V_c = 200$ m/min, $f = 0.15$ mm/rev, $w = 1.6$ mm, $\alpha = -7°$)

To evaluate the behavior of the thermal model based on the improved Oxley's theory, orthogonal cutting results obtained by Ivester et al. [25] were used. Experimental results include maximum temperature values at the tool/chip interface. The estimated maximum temperatures at the tool/chip interface were compared with the experimental results in Table 4. Considering the improved Oxley's machining model, the temperature values on the chip and tool sides were acquired to be close to the experimental results in most cases. The highest temperature percentage errors were −16.6 and −23.1 % for the chip and tool, respectively. It was found from the table that the maximum temperatures were sensitive to an increase of the cutting speed and a better accuracy was obtained at the cutting speed $V_c = 300$ m/min. Generally, the improved Oxley's approach gave lower temperatures than the experimental tests. Because of the use the temperature-dependent thermal properties for the workpiece, the differences between the estimated chip temperatures and experimental temperature measurements were lower than the discrepancies between the obtained tool temperatures and the measured ones, except for the fourth and the last orthogonal cutting cases.

**Table 4** Estimated and measured interface temperatures

| Test | $V_c$ (m/min) | $f$ (mm/rev) | $\alpha$ (°) | Estimated maximum temperature increase (°C) | | Measured maximum temperature, $T_{M,int}$ (°C) | $\varepsilon T_{int,c}$ (%) | $\varepsilon T_{int,t}$ (%) |
|---|---|---|---|---|---|---|---|---|
| | | | | $\Delta T_{M,c}$ | $\Delta T_{M,t}$ | | | |
| 1 | 200 | 0.15 | −7 | 1077.1 | 1020.1 | 1120 | −3.8 | −8.9 |
| 2 | 200 | 0.15 | 5 | 1042 | 961 | 1250 | −16.6 | −23.1 |
| 3 | 200 | 0.30 | −7 | 1214.5 | 1299.4 | 1100 | 10.4 | 18.1 |
| 4 | 200 | 0.30 | 5 | 1169.2 | 1193.4 | 1220 | −4.2 | −2.2 |
| 5 | 300 | 0.15 | −7 | 1165.4 | 1158.5 | 1310 | −11.0 | −11.6 |
| 6 | 300 | 0.15 | 5 | 1116.4 | 1063.7 | 1300 | −14.1 | −18.2 |
| 7 | 300 | 0.30 | −7 | 1283.3 | 1381.8 | 1305 | −1.7 | 5.9 |
| 8 | 300 | 0.30 | 5 | 1255.4 | 1310.4 | 1300 | −3.4 | 0.8 |

$\varepsilon T_{int,c} = \frac{\Delta T_{M,c} - T_{M,int}}{T_{M,int}} 100\ \%$ and $\varepsilon T_{int,t} = \frac{\Delta T_{M,t} - T_{M,int}}{T_{M,int}} 100\ \%$

## 5 Conclusions

Based on the process variables calculated using the improved Oxley's model that has the strain-hardening constant ($n_{eq}$), the temperature distributions in the chip, tool and workpiece were determined by considering the primary and secondary heat sources with border circumstances and imaginary heat sources. The presented thermal model involves heat transfer by conduction. With the use of imaginary sources, the adiabatic border circumstances are taken into account. The following points can be concluded:

1. Under all investigated cutting conditions, the convergent solution was obtained using the suggested initial values of the search parameters $\delta$, $C_0$ and $\phi$ for AISI 1045 steel.
2. Comparing the estimated results and the experimental data for orthogonal cutting of AISI 1045 steel, the value of the temperature factor $\eta$ was evaluated as 1, which helps to improve the estimation accuracy.
3. Compared to the extended Oxley's approach, the improved model for tool with negative rake angle resulted in more satisfactory values of cutting force, feed force and chip thickness that were closer to experimental results. The discrepancy between the results, calculated by the improved Oxley's model and obtained from experiments, was lesser than 8 % for cutting forces, 16 % for feed forces and 9 % for chip thicknesses. However, the feed forces obtained from the improved Oxley's model for tool with positive rake angle were significantly lower than those from experiments. The percentage errors in the feed force estimations indicate the need of further investigation.
4. The temperature increase in the workpiece generated by the primary heat source only was concentrated near the shear plane due to excessive deformation of the workpiece material for chip formation. Under the same cutting speed and feed rate, the average temperature increases in the chip around the primary heat source for tool with negative rake angle were greater than that for tool with positive rake angle. The temperature values were also sensitive to the cutting speed and feed rate. The average temperature values in the chip decreased with an increase in cutting speed and feed rate.
5. The maximum temperatures of the chip and tool sides at the tool/chip interface were found as close to the end of the tool/chip contact zone.
6. Through the thermal modeling of the united influence of the primary and secondary heat sources, it was found that the maximum temperature values estimated at the tool/chip interface were in satisfactory agreement with experimental results. The temperature distributions on the chip and tool sides at the tool/chip interface were also observed to be well matched.
7. The presented methodology demonstrates the effect of the improved Oxley's theory on the temperature distributions and gives a detailed understanding of the thermal process in machining. It can be utilized to design the cutting tool and optimize the process parameters.

## References


1. Budak E, Altıntaş Y, Armerago EJA (1996) Prediction of milling force coefficients from orthogonal cutting data. Trans ASME J Manuf Sci Eng 118:216–224
2. Aydın M, Uçar M, Cengiz A, Kurt M, Barkın B (2014) A methodology for cutting force prediction in side milling. Mater Manuf Process 29:1429–1435
3. Outeiro JC, Pina JC, M'Saoubi R, Pusavec F, Jawahir IS (2008) Analysis of residual stresses induced by dry turning of difficult-to-machine materials. CIRP Ann Manuf Technol 57:77–80
4. Lazoglu I, Altintas Y (2002) Prediction of tool and chip temperature in continuous and interrupted machining. Int J Mach Tools Manuf 42:1011–1022
5. Huang Y, Liang SY (2004) Modeling of CBN tool flank wear progression in finish hard turning transactions. Trans ASME J Manuf Sci Eng 126:98–106
6. Desai KA, Rao PVM (2012) On cutter deflection surface errors in peripheral milling. J Mater Process Technol 212:2443–2454
7. Aydın M, Uçar M, Cengiz A, Kurt M (2015) Identification of static surface form errors from cutting force distribution in flat-end milling processes. J Braz Soc Mech Sci 37:1001–1013
8. Özel T, Karpat Y (2005) Predictive modeling of surface roughness and tool wear in hard turning using regression and neural networks. Int J Mach Tools Manuf 45:467–479
9. Oxley PLB (1989) Mechanics of machining. An analytical approach to assessing machinability. Ellis Horwood Limited, Chichester
10. Adibi-Sedeh AH, Madhavan V, Bahr B (2003) Extension of Oxley's analysis of machining to use different material models. Trans ASME J Manuf Sci Eng 125:656–666
11. Johnson GR, Cook WH (1983) A constitutive model and data for metals subjected to large strains, high strain rates and high temperatures. In: The 7th international symposium on ballistics, Hague, Netherlands, pp 541–547
12. Özel T, Zeren E (2006) A methodology to determine work material flow stress and tool–chip interfacial friction properties by using analysis of machining. J Manuf Sci Eng 128:119–129
13. Lalwani DI, Mehta NK, Jain PK (2009) Extension of Oxley's predictive machining theory for Johnson and Cook flow stress model. J Mater Process Technol 209:5305–5312
14. Xiong L, Wang J, Gan Y, Li B, Fang N (2015) Improvement of algorithm and prediction precision of an extended Oxley's theoretical model. Int J Adv Manuf Technol 77:1–13
15. Huang Y, Liang SY (2003) Modelling of the cutting temperature distribution under the tool flank wear effect. Proc Inst Mech Eng C J Mech Eng Sci 217:1195–1208
16. Komanduri R, Hou ZB (2001) Thermal modeling of the metal cutting process. Part 1. Temperature rise distribution due to shear plane heat source. Int J Mech Sci 42:1715–1752
17. Komanduri R, Hou ZB (2001) Thermal modeling of the metal cutting process. Part 2. Temperature rise distribution due to

frictional heat source at the tool–chip Interface. Int J Mech Sci 43:57–88
18. Komanduri R, Hou ZB (2001) Thermal modeling of the metal cutting process. Part 3. Temperature rise distribution due to combined effects of shear plane heat source and the tool–chip interface frictional heat source. Int J Mech Sci 43:89–107
19. Karpat Y, Özel T (2006) Predictive analytical and thermal modeling of orthogonal cutting process. Part I. Predictions of tool forces, stresses, and temperature distributions. J Manuf Sci Eng 128:435–444
20. Huang Y, Liang SY (2003) Cutting forces modeling considering the effect of tool thermal property—application to CBN hard turning. Int J Mach Tools Manuf 43:307–315
21. Huang Y, Liang SY (2005) Cutting temperature modeling based on non-uniform heat intensity and partition ratio. Mach Sci Technol 9(3):301–323
22. Chen Y, Li H, Wang J (2015) Further development of Oxley's predictive force model for orthogonal cutting. Mach Sci Technol 19(1):86–111
23. Li L, Li B, Ehmann KF, Li X (2013) A thermo-mechanical model of dry orthogonal cutting and its experimental validation through embedded micro-scale thin film thermocouple arrays in PCBN tooling. Int J Mach Tools Manuf 70:70–87
24. Jaspers SPFC, Dautzenberg JH (2002) Material behaviour in conditions similar to metal cutting: flow stress in the primary shear zone. J Mater Process Technol 122:322–330
25. Ivester RW, Kennedy M, Davies M, Stevenson R, Thiele J, Furness R, Athavale S (2000) Assessment of machining models: progress report. Mach Sci Technol 4(3):511–538
26. Mathew P, Oxley PLB (1982) Predicting the effects of very high cutting speeds on cutting forces, etc. CIRP Ann Manuf Technol 31:49–52
27. Kato S, Yamaguchi K, Yamada M (1972) Stress distribution at the interface between tool and chip in machining. Trans ASME J Eng Ind 94:683–689
28. Usui E, Takeyama HA (1960) Photoelastic analysis of machining stresses. Trans ASME J Eng Ind 82:303–307
29. Zorev NN, Massey HSH (1966) Metal cutting mechanics. Pergamon Press, Oxford
30. Boothroyd G (1963) Temperatures in orthogonal metal cutting. Proc Inst Mech Eng 177(29):789–810